

Collective model for cluster motion in ${}^8\text{Be}$, ${}^{12}\text{C}$, and ${}^{16}\text{O}$ systems based on microscopic 2α , 3α , and 4α models

Yoshiko Kanada-En'yo

*Department of Physics, Kyoto University, Kyoto 606-8502, Japan*Nobuo Hinohara *Center for Computational Sciences, University of Tsukuba, Tsukuba 305-8577, Japan
and Faculty of Pure and Applied Sciences, University of Tsukuba, Tsukuba 305-8571, Japan*

(Received 18 July 2022; accepted 21 October 2022; published 10 November 2022)

A microscopic $n\alpha$ cluster model was applied to ${}^8\text{Be}$, ${}^{12}\text{C}$, and ${}^{16}\text{O}$ systems to investigate cluster motion in the ground state and radial excitation. In the microscopic calculation of ${}^{12}\text{C}$ and ${}^{16}\text{O}$ using the generator coordinate method with the coordinate D of the $\alpha - \alpha$ distance, excited states were obtained as the large-amplitude mode built on the ground state. A collective model was constructed to describe the cluster motion of these states by utilizing inputs from the microscopic cluster model such as the norm kernel and energy expectation values. Furthermore, the cluster model was extended by introducing the imaginary part of the coordinate D to incorporate the dynamical effects on the collective mass. The collective wave function obtained with the collective model was found to be in reasonable agreement with the results of the generator coordinate method for energies, root-mean-square radii, and amplitude functions.

DOI: [10.1103/PhysRevC.106.054312](https://doi.org/10.1103/PhysRevC.106.054312)

I. INTRODUCTION

In nuclear systems, large-amplitude collective motion plays an important role in various nuclear structure phenomena such as ground-state correlation, cluster excitation, and shape mixing, as well as in dynamical processes such as cluster decay and nuclear fission. To describe large-amplitude motion along a collective path in a microscopic framework, the generator coordinate method (GCM) [1,2] is one of the widely used approaches, particularly in the study of cluster phenomena [3–9]. However, application of the GCM is still limited to a few generator coordinates mainly because of the high computational cost of superposing a number of basis wave functions along the collective path, which requires non-diagonal elements of the microscopic Hamiltonian. To reduce the computational cost, semimicroscopic approaches, such as the orthogonality condition model [10] and phenomenological potential models, have been widely used in cluster physics. In many studies, potentials along the collective path are phenomenologically adjusted to fit existing data; however, they are not based on a fundamental derivation.

To derive the collective Hamiltonian by incorporating microscopic effects, various prescriptions have been proposed and are under development. One of the key problems is how to evaluate the collective mass in the kinetic term. However, as discussed in Ref. [11], some prescriptions, such as the cranking mass and Gaussian overlap approximation (GOA) mass [4,11] are known to be insufficient to quantitatively describe collective motion. The center-of-mass motion is a typical example that both prescriptions fail to describe. As a further microscopic approach to deriving the collective path

and collective Hamiltonian, the self-consistent collective coordinate method has been developed [12], and an adiabatic version has been applied to large-amplitude motion, including shape mixing and cluster phenomena [13–15]; however, it requires solving coupled equations.

In this study, we propose a convenient derivation of a collective model which can approximately describe the cluster dynamics obtained by the microscopic calculation of the GCM. We adopt the 2α , 3α , and 4α models for the ${}^8\text{Be}$, ${}^{12}\text{C}$, and ${}^{16}\text{O}$ systems, respectively. To describe cluster motion in the ground state and radial excitation, we use the Brink-Bloch cluster wave functions [3] with the most symmetric $n\alpha$ configurations, namely, the dumbbell, equilateral triangle, and regular tetrahedron configurations of 2α , 3α , and 4α , respectively. The $\alpha - \alpha$ distance is defined by parameter D , and the cluster motion along the coordinate D is considered. First, the ground and excited states are microscopically calculated by the GCM using the generator coordinate D , and the cluster motion in the obtained states is analyzed. Then, a collective model for the one-dimensional motion along the coordinate D is constructed by utilizing inputs from the microscopic $n\alpha$ wave functions, such as the norm kernel and energy expectation values, to derive the collective Hamiltonian. Moreover, to incorporate the dynamical effects on the collective mass, the microscopic cluster model is extended by introducing the imaginary part of the coordinate D . The collective Hamiltonian is evaluated by comparing the results for the energies, root-mean-square radii, and collective wave functions of the ground and excited states with the microscopic results obtained by the GCM.

This paper is organized as follows. Sections II and III describe the microscopic $n\alpha$ model and the microscopic Hamiltonian, respectively. The GCM results for the microscopic calculation are presented in Sec. IV, while the framework and results of the collective model are described in Sec. V. A summary is provided in Sec. VI. The Appendix presents a detailed derivation of the physical coordinates.

II. MICROSCOPIC $n\alpha$ CLUSTER MODEL

A. Wave functions of $n\alpha$ cluster system

A basis $n\alpha$ wave function is expressed by the Brink-Bloch α -cluster wave function [3,16] as

$$\Phi_{n\alpha}(\mathbf{S}_1, \dots, \mathbf{S}_n) = n_0 \mathcal{A}\{\psi_\alpha(\mathbf{S}_1) \cdots \psi_\alpha(\mathbf{S}_n)\}, \quad (1)$$

where \mathcal{A} is the antisymmetrizer, and $\psi_\alpha(\mathbf{S}_m)$ is the α -cluster wave function

$$\begin{aligned} \psi_\alpha(\mathbf{S}_m) &= \prod_{i \in \alpha_m} \phi_{S_m}(\mathbf{r}_i) \chi_i \tau_i, \\ \phi_{S_m}(\mathbf{r}_i) &= \left(\frac{2\nu}{\pi}\right)^{3/4} \exp[-\nu(\mathbf{r}_i - \mathbf{S}_m)^2], \end{aligned} \quad (2)$$

with the nucleon-spin and -isospin functions $\chi_i \tau_i$ selected as $p \uparrow$, $p \downarrow$, $n \uparrow$, and $n \downarrow$ for four nucleons $i = 4(k-1) + 1, \dots, 4(k-1) + 4$. The Gaussian width parameter ν is set to 0.235 fm^{-2} in the present calculation.

The parameter \mathbf{S}_m is usually treated as a real variable and indicates the mean center position of the m th α cluster (α_m) in the coordinate space before antisymmetrization in the original cluster model. However, complex variables for the Gaussian-center parameters \mathbf{S}_m are used in extended cluster models, as discussed in a later section.

To describe the intercluster motion in the GCM approach, the basis $n\alpha$ wave functions are superposed with respect to the generator coordinates \mathbf{S}_m as

$$\Psi_{\text{GCM}} = \int d\mathbf{S}_1, \dots, d\mathbf{S}_n f(\mathbf{S}_1, \dots, \mathbf{S}_n) \Phi_{n\alpha}(\mathbf{S}_1, \dots, \mathbf{S}_n), \quad (3)$$

where the coefficients $f(\mathbf{S}_1, \dots, \mathbf{S}_n)$ are determined by solving the Hill-Wheeler equation [1].

B. 2α , 3α , and 4α models for ${}^8\text{Be}$, ${}^{12}\text{C}$, and ${}^{16}\text{O}$ systems

1. Model space

In the 2α system for ${}^8\text{Be}$, we define the distance parameter $D = |\mathbf{S}|$ by taking $\mathbf{S}_1 = -\mathbf{S}_2 = \mathbf{S}/2$ and consider the relative motion between two α 's in one-dimensional model space with distance D .

To describe the ground states and radial excitation of the 3α and 4α systems for ${}^{12}\text{C}$ and ${}^{16}\text{O}$, we take highly symmetric configurations by setting the α -cluster positions in the equilateral triangle and regular tetrahedron configurations as illustrated in Fig. 1(b) and 1(c), respectively, and we describe the radial motion of α 's using the GCM approach. We define the $\alpha - \alpha$ parameter $D = |\mathbf{S}_m - \mathbf{S}_l|$ ($k \neq l$). Note that the radial distance $d = |\mathbf{S}_m|$ measured from the origin is obtained by scaling D as $d = D/2$, $D/\sqrt{3}$, and $\sqrt{3/8}D$, in the 2α , 3α ,

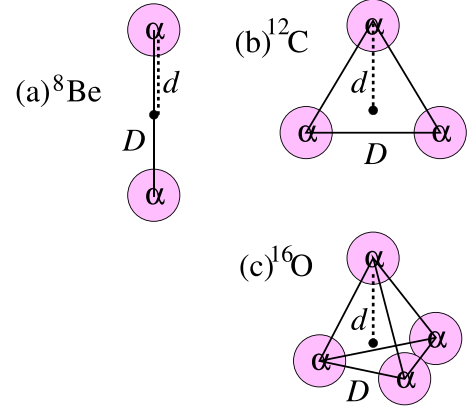


FIG. 1. Spatial configurations of the 2α , 3α , and 4α models for (a) ${}^8\text{Be}$, (b) ${}^{12}\text{C}$, and (c) ${}^{16}\text{O}$ systems.

and 4α systems, respectively. The GCM calculation with the coordinate D is equivalent to that with d .

2. GCM calculation

In the GCM calculation, the parity-projected wave functions $\Phi_{n\alpha}^\pm(D_j)$ at the mesh points of the coordinate D_j are superposed as

$$\Psi_k^\pm = \sum_j f_k^\pm(D_j) \Phi_{n\alpha}^\pm(D_j), \quad (4)$$

$$\Phi_{n\alpha}^\pm(D_j) \equiv \frac{\hat{P}^\pm \Phi_{n\alpha}(D_j)}{\langle \hat{P}^\pm \Phi_{n\alpha}(D_j) | \hat{P}^\pm \Phi_{n\alpha}(D_j) \rangle^{1/2}}, \quad (5)$$

where \hat{P}^\pm is the parity-projection operator. Sixteen mesh points $D_j = \{0.5 \text{ fm}, \dots, 8.0 \text{ fm}\}$ ($j = 1, \dots, 16$) with an interval of $\Delta_D = 0.5 \text{ fm}$ are used in the present calculations. The energy $E_{\text{GCM},k}^\pm$ and coefficients $f_k^\pm(D_j)$ for the k th parity(\pm) state are determined by diagonalization of the norm and Hamiltonian matrices

$$\mathcal{N}_{ij}^\pm = \langle \Phi_{n\alpha}^\pm(D_i) | \Phi_{n\alpha}^\pm(D_j) \rangle, \quad (6)$$

$$\mathcal{H}_{ij}^\pm = \langle \Phi_{n\alpha}^\pm(D_i) | \hat{H} | \Phi_{n\alpha}^\pm(D_j) \rangle. \quad (7)$$

For the GCM wave function Ψ_k^\pm obtained for the $(\pm)_k$ states, we define the amplitude function $G_{\text{GCM},k}^\pm(D_i)$ as

$$G_{\text{GCM},k}^\pm(D_i) \equiv \sum_j \{\mathcal{N}^{1/2}\}_{ij} f_k^\pm(D_j), \quad (8)$$

where $\mathcal{N}^{1/2}$ is the square root of the 16×16 matrix \mathcal{N}_{ij}^\pm in the basis space D_i ($i = 1, \dots, 16$). Since the norm kernel \mathcal{N}_{ij}^\pm is defined in a finite-size subspace $D_i \leq 8.0 \text{ fm}$ of the full D space, $G_{\text{GCM},k}^\pm(D_i)$ sometimes exhibits oscillatory behavior near the boundary $D_i \approx 8.0 \text{ fm}$ because of the finite-size effect; however, it is out our region of interest. We also calculate the overlap function $G_{\text{GCM},k}^{(2),\pm}(D_i)$ of Ψ_k^\pm with a basis wave function $\Phi_{n\alpha}^\pm(D_i)$ at D_i as

$$G_{\text{GCM},k}^{(2),\pm}(D_i) \equiv \langle \Phi_{n\alpha}^\pm(D_i) | \Psi_k^\pm \rangle = \sum_j \mathcal{N}_{ij}^\pm f_k^\pm(D_j). \quad (9)$$

TABLE I. Energies and root-mean-square radii (rmsr) calculated with the microscopic $n\alpha$ model of ${}^8\text{Be}$, ${}^{12}\text{C}$, and ${}^{16}\text{O}$. The values obtained by the generator coordinate method (GCM) and by single-basis calculation at the minimum-energy distance D_0 are presented in the second and third columns, respectively. The D_0 values are displayed in parentheses. For ${}^{12}\text{C}(+)$ and ${}^{16}\text{O}(+)$, the values of two-basis diagonalization for the small-amplitude calculation are presented in the fourth column.

	GCM E , rmsr (MeV), (fm)	Single E , rmsr(D_0) (MeV), (fm)	Small-amp. E , rmsr (MeV), (fm)
${}^8\text{Be}(+)_1$	-46.3, 2.67	-44.5, 2.37(3.2)	
${}^{12}\text{C}(+)_1$	-74.9, 2.35	-73.9, 2.31(2.2)	-73.8, 2.30
${}^{12}\text{C}(+)_2$	-60.1, 2.90		-52.8, 2.37
${}^{12}\text{C}(-)_1$	-67.8, 2.58	-66.7, 2.54(3.0)	
${}^{16}\text{O}(+)_1$	-127.1, 2.20	-126.7, 2.19(1.0)	-126.7, 2.19
${}^{16}\text{O}(+)_2$	-102.6, 2.46		-95.6, 2.24
${}^{16}\text{O}(-)_1$	-113.7, 2.34	-113.0, 2.31(1.7)	

Note that, owing to the orthonormality $\langle \Psi_k^\pm | \Psi_l^\pm \rangle = \delta_{kl}$, the amplitude function $G_{\text{GCM},k}^\pm(D_i)$ satisfies the orthonormal condition

$$\sum_i G_{\text{GCM},k}^{\pm*}(D_i) G_{\text{GCM},l}^\pm(D_i) = \delta_{kl}, \quad (10)$$

but the overlap function $G_{\text{GCM},k}^{(2),\pm}(D_i)$ does not. Considering the transformation $\Delta_D \sum_{D_i} \rightarrow \int dD$, we redefine the amplitude function $g_{\text{GCM},l}^\pm(D) \equiv G_{\text{GCM},l}^\pm(D)/\sqrt{\Delta_D}$ to satisfy the standard normalization in the coordinate D space as

$$\int g_{\text{GCM},k}^{\pm*}(D) g_{\text{GCM},l}^\pm(D) dD = \delta_{kl}. \quad (11)$$

III. MICROSCOPIC HAMILTONIAN

The microscopic Hamiltonian \hat{H} used in the present $n\alpha$ model consists of the single-nucleon kinetic energy, effective nucleon-nucleon (NN) forces, and NN Coulomb force. We use the effective central nuclear force given in a two-range Gaussian form of the Volkov No. 2 force [17] with the Majorana parameter $m = 0.62$, which has been used for cluster models in many studies. The total center of mass (cm) motion can be exactly separated, and its kinetic energy is subtracted from the Hamiltonian.

IV. RESULTS OF MICROSCOPIC CALCULATION

A. Energies and radii

The positive- and negative-parity states of ${}^8\text{Be}$, ${}^{12}\text{C}$, and ${}^{16}\text{O}$ were calculated by the GCM of the $n\alpha$ model. The results obtained for the energies and root-mean-square radii for the lowest $(\pm)_1$ and first excited states $(\pm)_2$ of each parity are presented in Table I. The calculated energy of the ${}^{16}\text{O}(+)_1$ state is in reasonable agreement with the experimental value $E^{\text{exp}}(\text{gs}) = -127.6$ MeV of the ${}^{16}\text{O}$ ground state, whereas the calculated energies of the ${}^8\text{Be}(+)_1$ and ${}^{12}\text{C}(+)_1$ states are more than 10 MeV higher than the experimental

values $E^{\text{exp}}(\text{gs}) = -56.50$ and -92.16 MeV, respectively. These binding energy defects can be partially explained by the energy gain due to the total angular momentum projection for ${}^8\text{Be}$ and ${}^{12}\text{C}$, and also by the spin-orbit attraction in ${}^{12}\text{C}$, neither of which is taken into account in the present $n\alpha$ model.

The lowest negative-parity states ${}^{12}\text{C}(-)_1$ and ${}^{16}\text{O}(-)_1$ correspond to the $K^\pi = 3^-$ bands because of the point-group symmetry of the triangle and tetrahedron configurations, respectively. The calculated excitation energy E_x of the ${}^{12}\text{C}(-)_1$ state, 7.1 MeV, is in reasonable agreement with the experimental value $E_x^{\text{exp}}(3_1^-) = 9.64$ MeV of the bandhead state, whereas that of ${}^{16}\text{O}(-)_1$, 13.4 MeV, overestimates the experimental value $E_x^{\text{exp}}(3_1^-) = 6.13$ MeV of the ${}^{16}\text{O}(3_1^-)$ state.

We also present the single-basis calculation results at the minimum-energy distance D_0 optimized for the diagonal elements of the Hamiltonian $E^\pm(D) = \langle \Phi_{n\alpha}^\pm(D) | \hat{H} | \Phi_{n\alpha}^\pm(D) \rangle$. A comparison of the single-basis and GCM results indicates that the ${}^{12}\text{C}(\pm)_1$ and ${}^{16}\text{O}(\pm)_1$ states can be approximately described by the single configuration at D_0 , whereas the ${}^8\text{Be}(+)_1$ state cannot be. This indicates that the $\alpha - \alpha$ motion in ${}^8\text{Be}(+)_1$ is not localized at a fixed distance, but exhibits large fluctuation along the generator coordinate D , which significantly increases the binding energy gain and radius of ${}^8\text{Be}(+)_1$ in the GCM calculation.

The first excited positive-parity states, ${}^{12}\text{C}(+)_2$ and ${}^{16}\text{O}(+)_2$, are radial excitations on the lowest states and have larger radii than the ${}^{12}\text{C}(+)_1$ and ${}^{16}\text{O}(+)_1$ states. The ${}^{12}\text{C}(+)_2$ and ${}^{16}\text{O}(+)_2$ states are associated with monopole excitation but cannot be assigned to the observed 0^+ states in the ${}^{12}\text{C}$ and ${}^{16}\text{O}$ spectra. These theoretical radial excitation modes may couple with other degrees of freedom, including α -cluster motion and single-particle excitation, and may be fragmented into several cluster states and also partially contribute to the giant monopole resonance. For ${}^8\text{Be}$, no excited state is obtained as a bound-state solution.

B. Potential energy curve and radial motion

To discuss the radial motion along the generator coordinate D , we present the potential energy curve $E^\pm(D)$, the GCM energies $E_{\text{GCM},k}^\pm$, and the GCM amplitude functions $g_{\text{GCM},k}^\pm(D)$ for the $(\pm)_1$ and $(\pm)_2$ states in Fig. 2.

In ${}^8\text{Be}$, the energy curve displays effective repulsion in the interior region because of the antisymmetrization effect and a shallow energy pocket at $D \approx 3$ fm. The GCM amplitude $g_{\text{GCM},1}^+(D)$ is spread widely around the energy minimum. As the number n of α clusters increases in ${}^{12}\text{C}$ and ${}^{16}\text{O}$, the energy pocket increases and shifts toward the interior region. Consequently, the amplitude $g_{\text{GCM},1}^+$ of the ${}^{12}\text{C}(+)_1$ state is drawn inward, and that of the ${}^{16}\text{O}(+)_1$ state concentrates around $D \approx 0$ to form a compact 4α state, which approximately corresponds to the p -shell closed state. For the excited positive-parity states $(+)_2$ of ${}^{12}\text{C}$ and ${}^{16}\text{O}$, one can observe nodal behavior of $g_{\text{GCM},2}^+$ exhibiting vibration features of the radial (D) excitation built on the lowest states.

For the negative-parity states, the potential energy increases particularly in the interior region, and the energy minima slightly shift outward. Moreover, the amplitudes $g_{\text{GCM},k}^-$ shift somewhat outward, but they show qualitatively

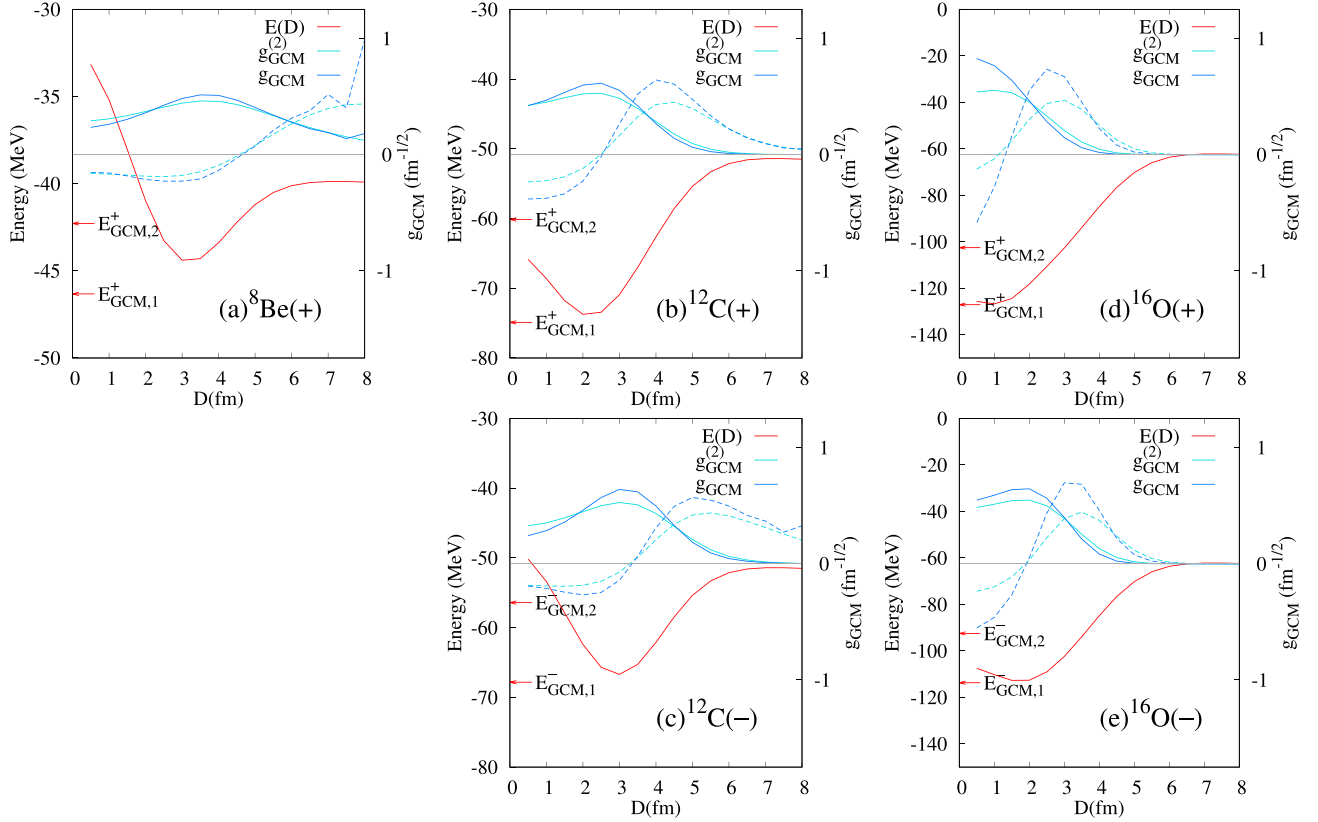


FIG. 2. GCM results of the energy curves $E^\pm(D)$, GCM energies $E_{\text{GCM},k}^\pm$, and GCM amplitude functions $g_{\text{GCM},k}^\pm(D)$ for (a) ${}^8\text{Be}(+)$, (b) ${}^{12}\text{C}(+)$, (c) ${}^{12}\text{C}(-)$, (d) ${}^{16}\text{O}(+)$, and (e) ${}^{16}\text{O}(-)$. For comparison, scaled values of the overlap function, $g_{\text{GCM},k}^{(2),\pm}(D) = cG_{\text{GCM},k}^{(2),\pm}(D)$, are also shown. Solid (dashed) lines indicate the amplitude and overlap functions of lower (\pm)₁ [higher (\pm)₂] states.

similar features to the positive-parity states. In other words, the amplitudes for the $(-)$ ₁ states concentrate around the energy minima and those for the $(-)$ ₂ states exhibit the features of the vibrational excitation constructed on the $(-)$ ₁ states along D .

These results support the possible interpretation of the GCM amplitude $g_{\text{GCM},k}^\pm$ as “collective wave functions” in the collective coordinate D for the (\pm) _{1,2} states. It should be noted that, although $g_{\text{GCM},k}^\pm$ satisfies the orthonormal condition (11) for the D integral, it does not satisfy the negative-parity boundary condition $g_{\text{GCM}}^-(0) = 0$ naively expected from the transformation $g_{\text{GCM}}^-(D) = -g_{\text{GCM}}^-(-D)$. It is indicated that the boundary condition at $D = 0$ of the collective wave function is not trivial because of the strong microscopic effects in the interior region close to $D = 0$.

Figure 2 also displays the overlap function $G_{\text{GCM},k}^{(2),\pm}(D)$ given in Eq. (9). To compare it with the amplitude function, we plot scaled values $g_{\text{GCM},k}^{(2),\pm} \equiv cG_{\text{GCM},k}^{(2),\pm}$ with a factor $c = (\frac{2\nu 4(A-4)}{A\pi})^{1/4}$, as performed in Ref. [18] to evaluate intercluster wave functions from the norm overlap. The D dependence of the overlap function $g_{\text{GCM},k}^{(2),\pm}$ is qualitatively consistent with that of the amplitude function $g_{\text{GCM},k}^\pm$ at least for the peak and node positions. This result indicates that $|g_{\text{GCM},k}^{(2),\pm}(D)|^2$ can be an alternative quantity for the probability at D as expected from the physical meaning of the overlap. However, it should be kept in mind that neither $g_{\text{GCM},k}^{(2),\pm}(D)$ nor $G_{\text{GCM},k}^{(2),\pm}(D)$

satisfies the orthonormal condition, which may be a significant problem in associating them with a kind of “collective wave function.”

V. COLLECTIVE MODEL

The aim of this section is to construct a potential model for the collective motion along the parameter D in $n\alpha$ systems. The key question is how to derive a collective Hamiltonian that can approximately describe the microscopic results obtained by the GCM. For this purpose, we first describe the antisymmetrization effects on the coordinate space of D in the microscopic wave function, and consider an extension of the real parameter D to a complex variable to discuss the dynamical effects on the cluster motion. Then we propose a collective Hamiltonian for the cluster motion. Finally, we present the results obtained by solving the collective Hamiltonian, and compare them with the GCM results.

A. Antisymmetrization effect on collective coordinate distance D

1. Physical meaning of D

In the asymptotic region, where the antisymmetrization effect vanishes, the parameter D corresponds to the mean distance between α positions. However, this is not the case in the small D region in which D no longer has the phys-

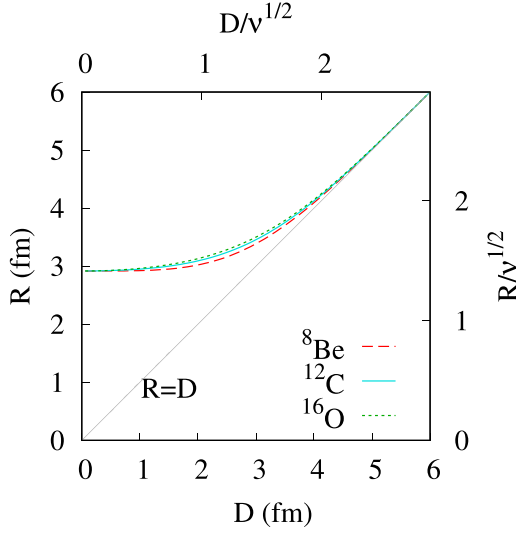


FIG. 3. Physical coordinates R plotted as functions of D for the $n\alpha$ wave functions.

ical meaning of the intercluster distance because of the antisymmetrization effect between α clusters. To demonstrate this antisymmetrization effect, we follow the prescription for the transformation of coordinates proposed by Ono *et al.* [19]. Ono *et al.* transformed a set of Gaussian centers $\{\mathbf{Z}_i\}$ of single-nucleon wave functions into a new set of coordinates $\{\mathbf{W}_i\}$ in the framework of antisymmetrized molecular dynamics (AMD). They call the new coordinates $\{\mathbf{W}_i\}$ “physical coordinates” and used them to avoid Pauli blocking in time-dependent AMD to study heavy-ion collision. A detailed derivation of the new coordinates $\{\mathbf{W}_i\}$ is provided in the Appendix. In the case of the present $n\alpha$ model at a given value of D , \mathbf{W}_i is analytically given as $\mathbf{W}_i = \lambda_{n\alpha}(D)\mathbf{Z}_i$ with the scaling factor $\lambda_{n\alpha}(D)$. According to this transformation, the parameter D is transformed into a new coordinate $R = \lambda_{n\alpha}(D)D$, which can be regarded as a “physical coordinate” for the $\alpha - \alpha$ distance. Figure 3 shows $R(D)$ for the 2α , 3α , and 4α systems. The D dependence of R shows almost no system dependence, indicating that the antisymmetrization effect between two α 's is essential for $R(D)$. In all cases, R takes the minimum value of $\sqrt{2}/v$ in the $D \rightarrow 0$ limit, signifying that two α 's cannot come closer to each other due to the Pauli blocking between identical nucleons in two α 's. As D increases, R monotonically increases and approaches $R \rightarrow D$ in the $D \gtrsim 5$ fm region.

2. Norm overlap and metric

The norm kernel $\mathcal{N}(D, D')$ of the 2α system is given as

$$\begin{aligned} \mathcal{N}(D, D') &= \langle \Phi_{2\alpha}(D) | \Phi_{2\alpha}(D') \rangle \\ &= \left[e^{-v \frac{(D'-D)^2}{4}} - e^{-v \frac{(D'+D)^2}{4}} \right]^4. \end{aligned} \quad (12)$$

In the asymptotic region of large D , the $\alpha - \alpha$ relative motion is not affected by antisymmetrization and is expressed by a Gaussian function of the relative coordinate r as $e^{-v_D(r-D)^2}$, where $v_D = 4 \times 4v/(4+4)$. Consequently, $\mathcal{N}(D, D')$ for

$\epsilon \equiv D' - D$ becomes a Gaussian function as

$$\mathcal{N}(D, D + \epsilon) \rightarrow e^{-\frac{v_D}{2}\epsilon^2}, \quad (13)$$

which satisfies the Gaussian overlap with constant width v_D . The parameter v_D is the metric adopted in the GOA. It turns out that the norm kernel can be used as a measure to evaluate the number of states contained in the small interval ϵ of the parameter space and the metric is expressed by the leading ϵ^2 term of $1 - \mathcal{N}(D, D + \epsilon)$ according to the ϵ^2 expansion:

$$1 - \mathcal{N}(D, D + \epsilon) \rightarrow \frac{v_D}{2}\epsilon^2 + \mathcal{O}(\epsilon^4). \quad (14)$$

We naively extend the prescription of this asymptotic feature of the norm kernel and introduce a D -dependent metric $\gamma_N(D)$ as

$$\gamma_N(D) \equiv \frac{1 - \mathcal{N}(D, D + \epsilon)}{(v_D/2)\epsilon^2}, \quad (15)$$

where $\gamma_N(D)$ is normalized to v_D to approach $\gamma_N(D) \rightarrow 1$ in the asymptotic region.

In the present calculation, we consider the parity-projected $n\alpha$ wave function at D denoted as $|D\rangle = |\Phi_{n\alpha}^\pm(D)\rangle$ and redefine $\gamma_N(D)$ for the $n\alpha$ systems in the general form with the norm kernel $\mathcal{N}^\pm(D, D') = \langle D | D' \rangle$ as

$$\gamma_N(D) \equiv \frac{1 - \mathcal{N}^\pm(D, D + \epsilon)}{1 - \mathcal{N}^\pm(D_\infty, D_\infty + \epsilon)}, \quad (16)$$

where the denominator is the asymptotic value in the $D \rightarrow \infty$ limit. Figure 4 shows the calculated values of $\gamma_N(D)$ for ${}^8\text{Be}(+)$, ${}^{12}\text{C}(\pm)$, and ${}^{16}\text{O}(\pm)$. In the $D > 5$ fm region, $\gamma_N \approx 1$, indicating that the antisymmetrization effect almost vanishes in this region.

In the $D \lesssim 5$ fm region, γ_N becomes smaller than 1 as D decreases and finally approaches zero at the $D \rightarrow 0$ limit because of the antisymmetrization effect. In ${}^{12}\text{C}$ and ${}^{16}\text{O}$, one can see a significant parity dependence of γ_N . In particular, γ_N in ${}^{16}\text{O}(+)$ exhibits unnatural oscillating behavior due to the parity-projection effect. The intrinsic wave function of 4α before parity projection is a mixed-parity state for $D \neq 0$, but it is a pure positive-parity state in the $D \rightarrow 0$ limit. In the small- D region, the shift $D \rightarrow D + \epsilon$ involves a drastic change of the parity mixing ratio, which has a nontrivial effect on γ_N via $\mathcal{N}^\pm(D, D')$ calculated using the parity-projected wave function. In other words, the nontrivial parity dependence of γ_N originates from the quantum effect associated with the parity symmetry restoration.

Let us discuss the behavior of $R' \equiv dR/dD$ of the physical coordinate R . Provided that the metric is constant in the coordinate space of R , $(R')^2$ is naively expected to be an alternative metric. In Fig. 4, the values of R' and $(R')^2$ are compared with γ_N . $(R')^2$ is strongly suppressed in the $D \lesssim 5$ fm region, and inconsistent with γ_N . However, R' is in a better agreement with γ_N but does not describe the parity dependence of γ_N in ${}^{12}\text{C}$ and ${}^{16}\text{O}$.

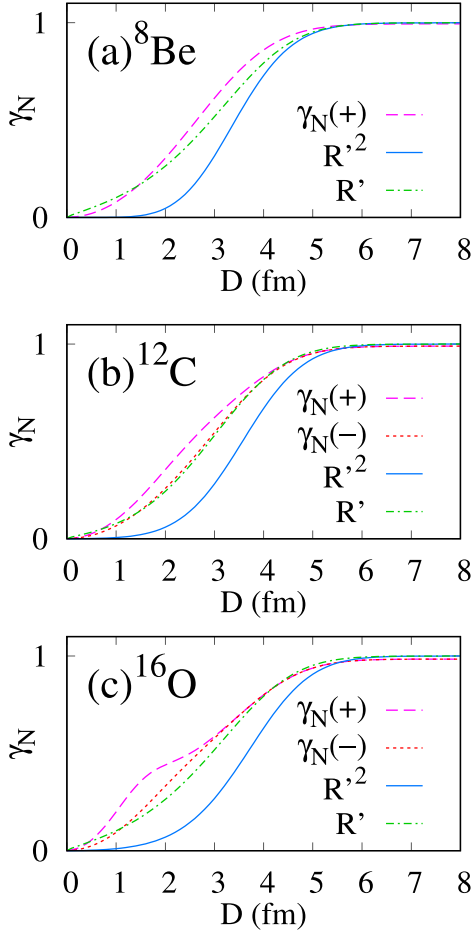


FIG. 4. γ_N derived from the norm kernel $\mathcal{N}(D, D')$ for (a) ${}^8\text{Be}(+)$, (b) ${}^{12}\text{C}(\pm)$, and (c) ${}^{16}\text{O}(\pm)$. For comparison, $R' = dR/dD$ and $(R')^2$ obtained from the physical coordinate R are also shown.

B. $n\alpha$ systems with complex parameter

We extend the $n\alpha$ wave function by introducing the imaginary part of the coordinate D as $D \rightarrow D + iP/(2\hbar v)$. This extension is achieved by using the complex parameter for the Gaussian centers instead of the real parameter D . For instance, in the case of 2α , the extended $n\alpha$ wave function is given by replacing the real parameter $S = (0, 0, D)$ for the Gaussian centers $S_1 = -S_2 = S/2$ of two α 's as $S = (0, 0, D + \frac{iP}{2\hbar v})$.

The real parameter P introduced here corresponds to an imaginary shift of D , and the $n\alpha$ state $|D, P\rangle$ can be written as

$$|D, P\rangle = n_0(D, P)e^{i\frac{P}{2\hbar v}\frac{\partial}{\partial D}}|D\rangle, \quad (17)$$

where n_0 is the normalization factor determined so that $\langle D, P|D, P\rangle = 1$. Note that the operator $e^{i\frac{P}{2\hbar v}\frac{\partial}{\partial D}}$ is not a unitary operator. Let us consider the 2α system. In the asymptotic region, where the antisymmetrization effect vanishes, the mean positions and momenta of nucleons are given as $\langle \mathbf{r}_i \rangle = (0, 0, \pm D/2)$ and $\langle \mathbf{p}_i \rangle = (0, 0, \pm P/2)$, respectively, while those of the relative motion between two α s are given as $\langle \mathbf{r} \rangle = (0, 0, D)$ and $\langle \mathbf{p} \rangle = (0, 0, \pm(\mu_{n\alpha}/M_N)P)$, respectively. Here $\mu_{n\alpha}$ is the reduced mass $\mu_{2\alpha} = M_N/2$ for the 2α systems. Indeed, the operator $e^{i\frac{P}{2\hbar v}\frac{\partial}{\partial D}}$ can be written using the boost

operators of nucleons with momenta $\pm P/2$ in the opposite direction with an D - and P -dependent overall factor. In a similar way, the reduced mass for the $n\alpha$ systems is defined as $\mu_{n\alpha} = (D/d)^2(M_N/A)$ using the nucleon mass M_N and $d = |\mathbf{S}_m|$.

We calculate the energy expectation value of the finite-momentum state $|D, P\rangle$ as

$$E_P = \langle D, P|\hat{H}|D, P\rangle, \quad (18)$$

and define the inverse mass $1/M_P(D)$ from the following relation,

$$\Delta E_P(D) = E_P(D) - E(D) = \frac{\hbar^2}{2M_P(D)}P^2, \quad (19)$$

where $E(D) = \langle D|\hat{H}|D\rangle$ is the energy at D and $P = 0$.

Figure 5 shows the P and D dependences of M_P . As shown in Fig. 5(a) for the P dependence, $M_P(D)$ is almost constant in the $P/\hbar \leq 0.3 \text{ fm}^{-1}$ region, and therefore we omit the P dependence of $M_P(D)$ in the following discussion. The D dependence of M_P at $P/\hbar = 0.05 \text{ fm}^{-1}$ for the positive- and negative-parity states is presented in Figs. 5(b) and 5(c), respectively. The values relative to the asymptotic value $\mu_{n\alpha}$ are plotted. In the $D > 5 \text{ fm}$ region, $M_P/\mu_{n\alpha}$ is approximately equal to 1, indicating that the antisymmetrization effect almost vanishes in this region. As D decreases, M_P increases in the $D \lesssim 5 \text{ fm}$ region. This increasing behavior of M_P seems inconsistent with the naive expectation that the antisymmetrization, i.e., the Pauli blocking effect, may give a repulsive effect and contributes to reducing the inertial mass of the kinetic term. As described above, M_P is measured by the inverse of the energy difference ΔE_P between two states $|D\rangle$ and $|D, P\rangle$. Since the antisymmetrization effect suppresses the state difference in the interior region, it contributes to decreasing the energy difference and increasing M_P . Therefore, it may not be adequate to directly use the obtained M_P values as the inertial mass of the collective model, but some modification may be necessary by taking into account the antisymmetrization effect.

C. Small-amplitude description

In the case of $P \neq 0$, the state $|D, P\rangle$ contains a component orthogonal to $|D\rangle$. However, in the $n\alpha$ model, the two-dimensional GCM using (D, P) obtains results consistent with the results of one-dimensional GCM with D for low-lying bound states, because the model space of (D, P) contains redundant states. Nevertheless, one of the advantages of introducing the complex parameter is that $|D, P\rangle$ provides a semiclassical picture of oscillation around the coordinate D in a simple expression of the single-basis wave function at (D, P) . In particular, the $\mathcal{O}(P)$ term of $|D, P\rangle$ involves the time-odd components for the small-amplitude mode around the static solution $|D\rangle$.

To discuss the vibration feature of the radial excitation in the ${}^{12}\text{C}$ and ${}^{16}\text{O}$ systems, we take a small value of $P/\hbar = 0.1 \text{ fm}^{-1}$ at the optimized D_0 for the energy minimum of $E(D)$, and diagonalize two bases of the time reversal partners,

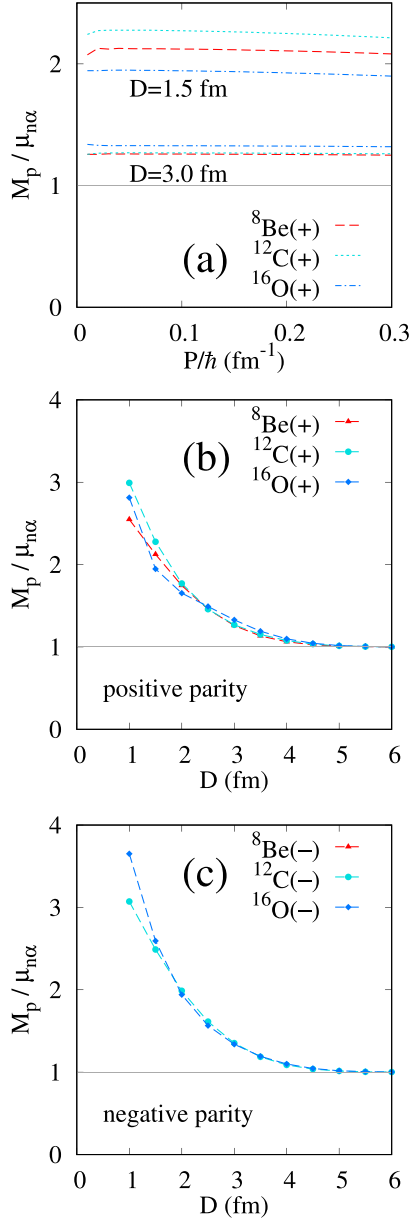


FIG. 5. Mass M_p evaluated by $|D, P\rangle$ with the complex parameter $D + iP/(2\hbar\nu)$. (a) P dependence of M_p at $D = 1.5$ and 3.0 fm, (b) D dependence of M_p for positive-parity states, and (c) D dependence of M_p for negative-parity states. The values are divided by the asymptotic value $\mu_{n\alpha} = (D/d)^2(M_N/A)$ of $n\alpha$ systems.

$|D_0, P\rangle$ and $|D_0, -P\rangle$, to obtain a small-amplitude oscillation in the ground and excited states, $\Psi_{s\text{-amp},k}^\pm$. The results obtained by the two-basis diagonalization for the small-amplitude approximation are shown in the fourth column of Table I for the energy and radii, and in Fig. 6 for the overlap function $G_{s\text{-amp},k}^{(2),\pm}(D) \equiv \langle \Phi_{n\alpha}^\pm(D) | \Psi_{s\text{-amp},k}^\pm \rangle$. Compared with the GCM calculation, the small-amplitude calculation tends to overestimate the energies and underestimate the radii, indicating that these states obtained by the GCM are not small-amplitude vibrations but large-amplitude motion. In particular, significant differences from the GCM results are obtained for the

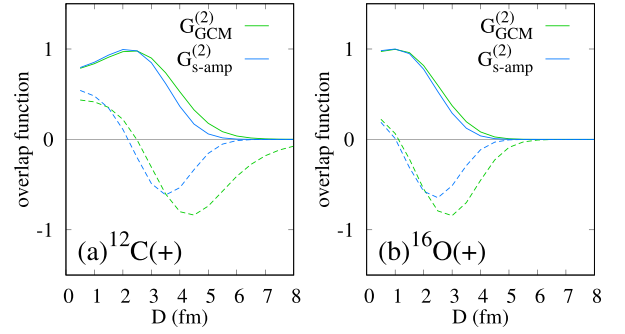


FIG. 6. Overlap function $G_{s\text{-amp},k}^{(2),\pm}$ obtained by two-basis diagonalization for the small-amplitude calculation of (a) $^{12}\text{C}(+)$ and (b) $^{16}\text{O}(+)$. The GCM results of the overlap function, $G_{\text{GCM},k}^{(2),\pm}$, are also shown for comparison. Solid (dashed) lines indicate the overlap functions of lower $(\pm)_1$ [higher $(\pm)_2$] states.

excited states shown in Fig. 6. An exception is the $^{16}\text{O}(+)_1$ state, which is well reproduced by the small-amplitude approximation.

D. Collective Hamiltonian

In general, it is difficult for nonmicroscopic potential models to obtain results equivalent to microscopic calculations. Nevertheless, semimicroscopic or phenomenological potential models are useful to obtain reasonable results and are widely applied to study the dynamics of cluster motion. The aim of this section is to construct a collective Hamiltonian that can approximately describe the fundamental properties of the cluster motion in the ground and excited states obtained by the microscopic calculation of the GCM. At small D , the microscopic state $|D\rangle$ is a highly nonlocalized state and contains strong quantum effects such as antisymmetrization and parity projection, and therefore the GOA is not applicable. We consider an alternative approach as follows.

The basic idea is that we assume local collective variables in the collective Hamiltonian by utilizing diagonal elements, i.e., expectation values of microscopic operators \hat{O} obtained by a single basis of the microscopic $n\alpha$ model wave function. This signifies that nontrivial microscopic effects, such as the antisymmetrization and parity projection, are taken into account as local inputs as much as possible. In the asymptotic region, D , $M_p(D)$, and $g_{\text{GCM},k}^\pm(D)$ can be regarded as the collective coordinate, mass, and collective wave function of the radial motion of the $n\alpha$ systems. Indeed, D and $M_p(D)$ satisfy the asymptotic conditions $\langle r \rangle \rightarrow D$ and $M_p \rightarrow \mu_{n\alpha}$, respectively. Moreover, $|g_{\text{GCM},k}^\pm(D)|$ represents the probability, and $g_{\text{GCM},k}^\pm(D)$ satisfies the orthonormal condition in the coordinate D space as given in Eq. (10). We start from the collective Hamiltonian with the collective coordinate D space and the mass M_p by taking into account the metric in the D space, and consider several options. Then we solve the eigenvalue problem of the collective model and evaluate whether it provides results in reasonable agreement with the microscopic results of the GCM.

We assume that the collective Hamiltonian consists of the kinetic and potential terms as

$$\mathcal{H}_{\text{coll}} = \mathcal{T}_{\text{coll}} + \mathcal{V}_{\text{coll}}(D), \quad (20)$$

and suppose that it can approximately describe energies $E_{\text{GCM},k}^{\pm}$ and collective wave functions $g_{\text{GCM},k}^{\pm}(D)$. For the potential term, we adopt a parity-dependent local potential of $\mathcal{V}_{\text{coll}}(D) = E^{\pm}(D) - T_0$, where T_0 is a constant value of $T_0 = \hbar\omega/4$ ($\omega = 2\hbar^2\nu/M_N$) for the zero-point energy contained in the microscopic $n\alpha$ wave function at a large D .

In general, the coordinate D space has a metric $\gamma(D)$, and observables for local operators $\mathcal{O}_{\text{coll}}$ in the D space are given by the expectation values using the collective wave function $\Phi_{\text{coll}}(D)$ and the weight factor $\sqrt{\gamma}$ as

$$\langle \mathcal{O}_{\text{coll}} \rangle = \int \Phi_{\text{coll}}^*(D) \mathcal{O}_{\text{coll}}(D) \Phi_{\text{coll}}(D) \sqrt{\gamma} dD. \quad (21)$$

Following a prescription for quantization in one dimension with the metric γ , we introduce the kinetic term of $\mathcal{H}_{\text{coll}}$ as

$$\mathcal{T}_{\text{coll}} = -\frac{\hbar^2}{2} \frac{1}{\sqrt{\gamma}} \frac{d}{dD} \sqrt{\gamma} \frac{1}{\gamma\mu} \frac{d}{dD}, \quad (22)$$

The microscopic effects are taken into account in the D dependence of γ and μ , but in the asymptotic region they should be constant as $\gamma \rightarrow 1$ and $\mu \rightarrow \mu_{n\alpha}$ so that the kinetic term takes the standard form,

$$\mathcal{T}_{\text{coll}} \rightarrow -\frac{\hbar^2}{2\mu_{n\alpha}} \frac{d^2}{dD^2} \quad (D \rightarrow \infty). \quad (23)$$

For the metric γ and mass μ in the collective model, we consider five cases as follows. In the first case (1), we adopt the D -dependent metric and mass as $\gamma = \gamma_N(D)$ and $\mu = M_P(D)$, which are obtained by utilizing the norm kernel $\mathcal{N}(D, D')$ and the finite-momentum state $|D, P\rangle$. Note that $\gamma_N(D)$ and $M_P(D)$ are parity dependent as they are obtained with the parity-projected $n\alpha$ wave function as mentioned previously. In the second case (2), $\gamma = 1$ is kept constant, and we use the mass $\mu = \gamma_N(D)M_P(D)$. In the third case (3), we use the mass $\mu = M_P(D)$ and take an alternative metric derived from the physical coordinate $R(D)$ as $\gamma = dR/dD \equiv \gamma_R$. In this case, μ is parity dependent, but γ is not. The fourth case (4) is a reference case; we use the naive ansatz of the constant values $\gamma = 1$ and $\mu = \mu_{n\alpha}$. We also perform a test calculation in the fifth case (5) using $\gamma = 1$ and $\mu = M_P(D)$. It should be noted that all cases satisfy the asymptotic conditions.

In Table II, we summarize the five sets of γ and μ in the collective model, which are labeled cal(1) to cal(5). In the table, the notations γ_N^{\pm} and M_P^{\pm} are used to explicitly denote the parity dependence of γ_N and M_P . It should be noted that the D -dependent γ incorporates the microscopic effects on the coordinate D space from the microscopic wave function, but not the dynamical effect from the microscopic Hamiltonian. However, M_P in the kinetic term and the potential term $\mathcal{V}_{\text{coll}}$ incorporate the dynamical effects in addition to the microscopic effects from the microscopic wave function.

TABLE II. Values of γ and μ used in the kinetic term Eq. (22) of the collective Hamiltonian $\mathcal{H}_{\text{coll}}$. The boundary condition of Φ_{coll}^- at $D = 0$ for negative-parity states is also listed; the default condition $\Phi_{\text{coll}}^-(0) = 0$ in cal(1) to cal(5) and the optional condition $\Phi_{\text{coll}}^-(0) = 0$ in cal(1b) and cal(2b) cases, which are denoted as Φ' and Φ , respectively.

Default sets	cal(1)	cal(2)	cal(3)	cal(4)	cal(5)
μ	M_P^{\pm}	$\gamma_N^{\pm} M_P^{\pm}$	M_P^{\pm}	$\mu_{n\alpha}$	M_P^{\pm}
γ	γ_N^{\pm}	1	γ_R	1	1
$\Phi_{\text{coll}}^-(D=0)$	Φ'	Φ'	Φ'	Φ'	Φ'
Optional sets	cal(1b)	cal(2b)			
$\Phi_{\text{coll}}^-(D=0)$	Φ	Φ			

E. Collective wave function

The collective wave function $\Phi_{\text{coll}}(D)$ is obtained by solving the eigenvalue problem of the collective Hamiltonian $\mathcal{H}_{\text{coll}}$ in the coordinate space D under the orthonormal condition

$$\begin{aligned} \langle \Phi_{\text{coll}}(D) | \Phi_{\text{coll}}(D) \rangle \\ = \int \Phi_{\text{coll}}^*(D) \Phi_{\text{coll}}(D) \sqrt{\gamma} dD = 1. \end{aligned} \quad (24)$$

The obtained eigenvalue of the collective Hamiltonian is the energy of the collective state as follows:

$$\begin{aligned} \langle \Phi_{\text{coll}}(D) | \mathcal{H}_{\text{coll}} | \Phi_{\text{coll}}(D) \rangle \\ = \int \Phi_{\text{coll}}^*(D) \mathcal{H}_{\text{coll}} \Phi_{\text{coll}}(D) \sqrt{\gamma} dD. \end{aligned} \quad (25)$$

The root-mean-square radii are calculated with Eq. (21) by assuming that the collective operator $\mathcal{O}_{\text{coll}}(D)$ is given by the diagonal element (expectation value) of the microscopic wave function at D as

$$\mathcal{O}_{\text{coll}}(D) = \langle \Phi_{n\alpha}^{\pm}(D) | \sum_i (\hat{r}_i - \hat{r}_G)^2 | \Phi_{n\alpha}^{\pm}(D) \rangle, \quad (26)$$

where r_G is the total center of mass coordinate. We define $\phi_{\text{coll}}(D) \equiv \gamma^{1/4} \Phi_{\text{coll}}(D)$, which satisfies $\int \phi_{\text{coll}}^*(D) \phi_{\text{coll}}(D) dD = 1$ to compare the collective wave functions with the GCM solution $g_{\text{GCM}}^{\pm}(D)$.

The boundary condition of the collective wave function at $D = 0$ is not trivial because of the antisymmetrization effect. For positive-parity states, we set $d\Phi_{\text{coll}}^+(D)/dD = \Phi_{\text{coll}}^+(D) = 0$ at $D = 0$. For negative-parity states, the GCM amplitude function $g_{\text{GCM}}^-(D)$ is inconsistent with the standard condition $\Phi_{\text{coll}}^-(D) = 0$ of negative-parity states; that is, the parity transformation does not correspond to the transformation $g_{\text{GCM}}^{\pm}(D) \rightarrow g_{\text{GCM}}^{\pm}(-D)$ in the collective coordinate D space. Instead, we choose the condition $\Phi_{\text{coll}}^-(D) = 0$ at $D = 0$, with which we can obtain a better result than with the standard choice, as shown later. This condition corresponds to a calculation with the same condition as the positive-parity states but with the parity-dependent Hamiltonian. In other words, the parity-projection effects are incorporated in the Hamiltonian but not in the $D = 0$ boundary condition. In the asymptotic region, we adopt the same bound-state approximation used in the GCM calculation. Namely, the collective wave function

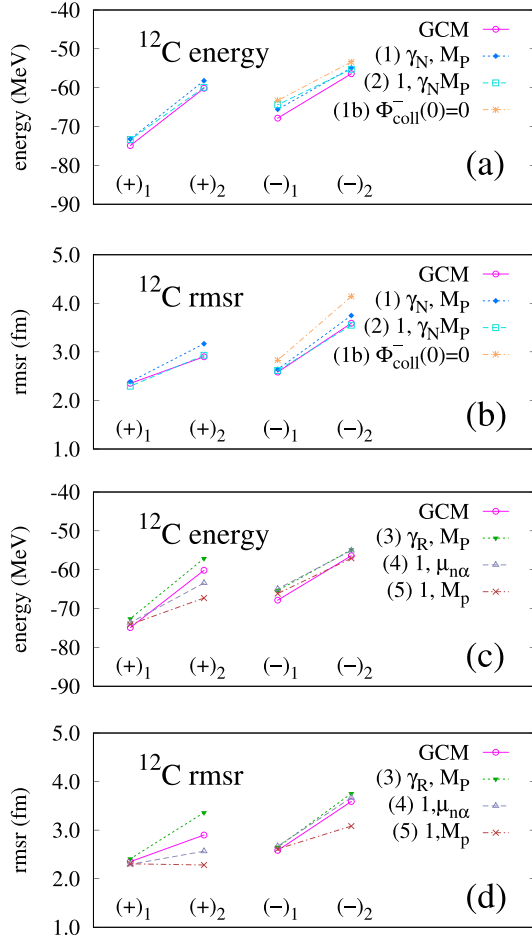


FIG. 7. Energies and radii (rmsr) of ^{12}C calculated by the collective models in comparison with the GCM results. This figure presents the results of cal(1), cal(2), and cal(1b) for the (a) energies and (b) radii, and the results of cal(3), cal(4), and cal(5) for the (c) energies and (d) radii.

is expressed by a sum of localized Gaussians with center positions from 0.5 to 8.0 fm with intervals of 0.5 fm, and the eigenvalue problem is solved by diagonalization.

F. Results of the collective Hamiltonian model

We show the results of the lowest and first excited states obtained by the collective model of the five cases and compare them with the microscopic results of the GCM. The results for the energies and radii of the $(+)_1,2$ and $(-)_1,2$ states of ^{12}C are shown in Fig. 7, while those of ^{16}O are shown in Fig. 8. As shown in Figs. 7(a), 7(b), 8(a), and 8(b), the collective model cal(1) using $\gamma = \gamma_N$ and $\mu = M_P$ reasonably reproduces the GCM result of the energies and radii of the lowest and excited states $^{12}\text{C}(\pm)_{1,2}$ and $^{16}\text{O}(\pm)_{1,2}$. The second model cal(2) using $\gamma = 1$ and $\mu = \gamma_N M_P$ produces results similar to the cal(1) results for ^{12}C and somewhat better results for ^{16}O .

Let us compare the results obtained by the optional case of the negative-parity boundary condition cal(1b) for $\Phi_{\text{coll}}^-(0) = 0$ with the cal(1) results for $\Phi_{\text{coll}}^-(0) = 0$. The former calculation (1b) overestimates the energies and radii of the GCM

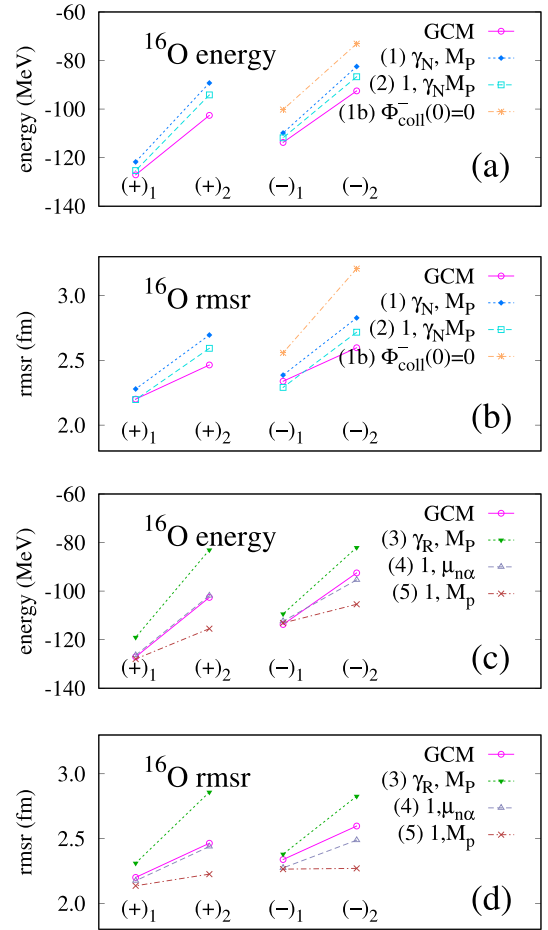


FIG. 8. Energies and radii (rmsr) of ^{16}O calculated by the collective models in comparison with the GCM results. This figure presents the results of cal(1), cal(2), and cal(1b) for the (a) energies and (b) radii, and the results of cal(3), cal(4), and cal(5) for the (c) energies and (d) radii.

results, indicating that the condition $\Phi_{\text{coll}}^-(0) = 0$ is not appropriate for the collective wave functions in the D space.

Other model calculations of cal(3), cal(4), and cal(5) are not satisfactory in systematically reproducing the GCM results [see Figs. 7(c), 7(d), 8(c), and 8(d)]. In particular, these calculations failed to reproduce the properties of the $^{12}\text{C}(+)_{2}$ state, and the calculations of cal(3) and cal(5) cannot describe the radii of the $^{12}\text{C}(+)_{2}$ and $^{16}\text{O}(+)_{2}$ states, because the metric γ_R used in cal(3) is slightly smaller than γ_N for the positive-parity states and provides a stronger repulsive effect in the kinetic term than that in the case of cal(1). Compared with cal(3) and cal(5), improved results are obtained by cal(4) for some states. However, the results of cal(4) do not show global reproductions but the agreement is state and system dependent. Therefore, the sets of γ and μ used in these models do not work for describing the collective motion along D in the $n\alpha$ systems.

We compare the results obtained by cal(4) and cal(5) with those of cal(2). These three calculations use the constant metric $\gamma = 1$ but different values of the collective mass in

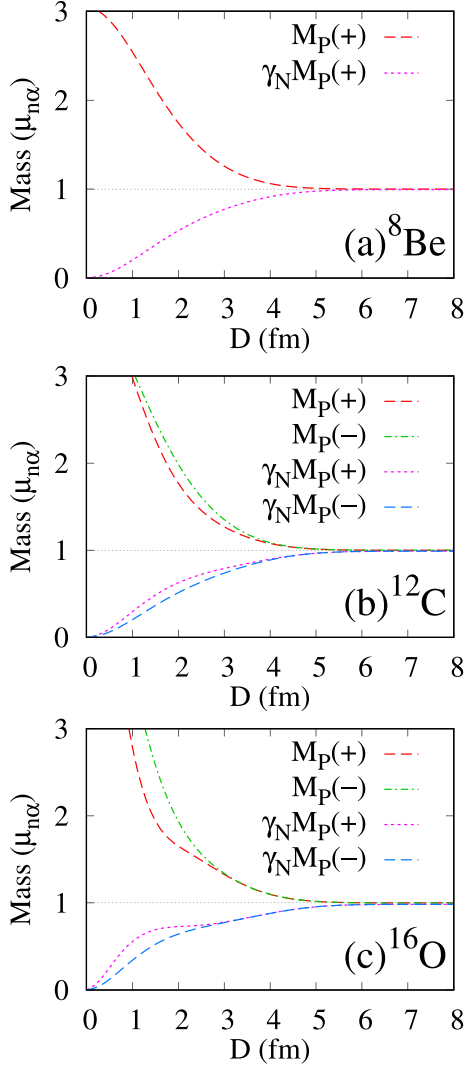


FIG. 9. D dependences of the inertial mass $\mu = M_P$ and $\gamma_N M_P$ used in cal(5) and cal(2) for (a) ${}^8\text{Be}(+)$, (b) ${}^{12}\text{C}(\pm)$, and (c) ${}^{16}\text{O}(\pm)$. The values relative to the constant mass $\mu = \mu_{n\alpha}$ corresponding to cal(4) are plotted.

the kinetic term: $\mu = \gamma_N M_P$, $\mu_{n\alpha}$, and M_P are used in cal(2), cal(4), and cal(5), respectively. Figure 9 shows the D dependence of μ of cal(2) and cal(5) relative to the constant mass $\mu_{n\alpha}$ for cal(4). In the interior region, $\mu = \gamma_N M_P$ for cal(2) is suppressed because of the antisymmetrization effect, whereas $\mu = M_P$ for cal(5) is enhanced.

Here, cal(4) underestimates the radius of the ${}^{12}\text{C}(+)_2$ state because the constant γ and μ values of cal(4) provide no repulsive effect in the kinetic term compared with the case of cal(2). The model cal(5) significantly underestimates the radii of all states of ${}^{16}\text{O}$ as well as the ${}^{12}\text{C}(\pm)_2$ states because $\mu = M_P$, which is largely enhanced in the interior region, provides more attractive effects compared with the cases cal(2) and cal(4).

To examine the behavior of the collective motion in greater detail, Fig. 10 exhibits the collective wave functions ϕ_{coll} obtained by the collective models of cal(1) and cal(2) compared

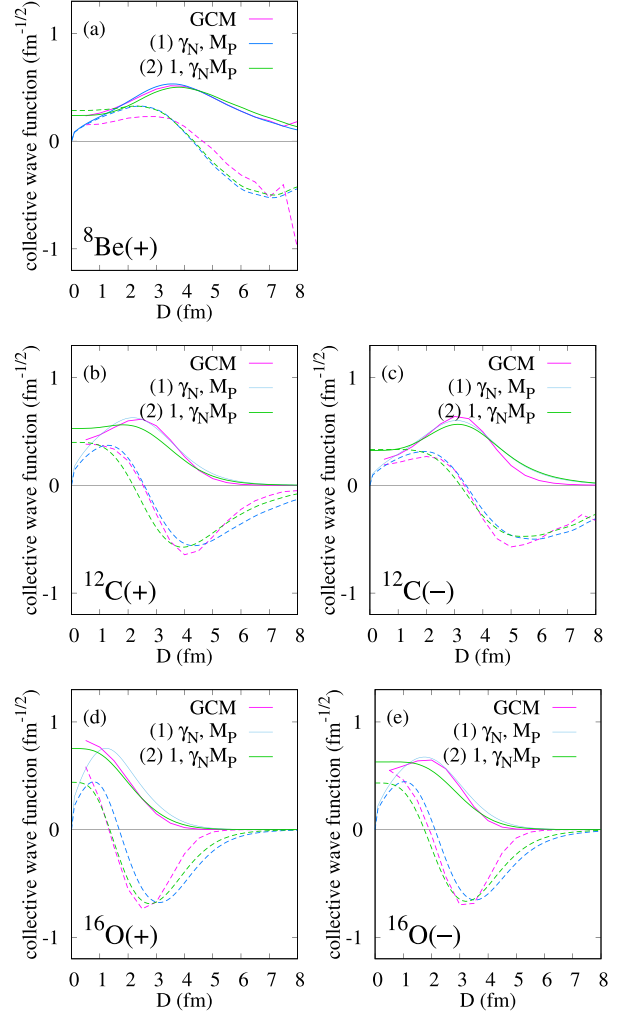


FIG. 10. Collective wave functions $\phi_{\text{coll}}(D)$ calculated by the collective models of cal(1) and cal(2) compared with the GCM amplitude function $g_{\text{GCM}}^{\pm}(D)$. The results are displayed for (a) ${}^8\text{Be}(+)$, (b) ${}^{12}\text{C}(+)$, (c) ${}^{12}\text{C}(-)$, (d) ${}^{16}\text{O}(+)$, and (e) ${}^{16}\text{O}(-)$. Solid (dashed) lines indicate the functions of lower $(\pm)_1$ [higher $(\pm)_2$] states.

with the GCM amplitude function g_{GCM}^{\pm} . Although the same boundary condition at $D = 0$ is adopted for $\Phi_{\text{coll}}(D)$ in cal(1) and cal(2), $\phi_{\text{coll}}(D) = \gamma^{1/4} \Phi_{\text{coll}}(D)$ has different behavior at $D = 0$. In the case of cal(1), an additional node appears in ϕ_{coll} at $D = 0$, because $\gamma_N(D) \rightarrow 0$ in the $D \rightarrow 0$ limit, but not in the case of cal(2). Because of this additional node, ϕ_{coll} of cal(1) slightly shifts outward compared with the cal(2) result. In particular, in the ${}^{16}\text{O}(+)$ states, the result of cal(1) fails to describe the concentration around $D \approx 0$ of the GCM amplitude in the deep potential, because the $D = 0$ node prevents ϕ_{coll} from penetrating in the short distance region [see Fig. 10(d)].

In principle, $\phi_{\text{coll}}(D)$ of cal(1) and cal(2) are similar to each other except for the $D = 0$ node in cal(1), which does not satisfy our requirement of reproducing the GCM amplitude function. The set of $\gamma = 1$ and $\mu = \gamma_N M_P$ in cal(2) is a simple prescription to effectively take into account the

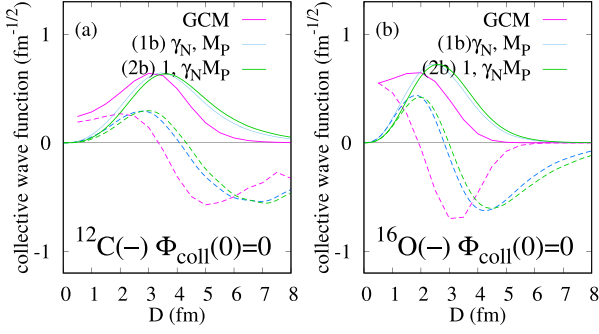


FIG. 11. Collective wave functions $\phi_{\text{coll}}(D)$ calculated by the collective models cal(1b) and cal(2b) for the optional case of the negative-parity boundary condition $\Phi_{\text{coll}}^-(0) = 0$, in comparison with the GCM amplitude function $g_{\text{GCM}}^\pm(D)$. The results for (a) $^{12}\text{C}(-)$ and (b) $^{16}\text{O}(-)$. Solid (dashed) lines indicate the functions of lower ($-$)₁ [higher ($-$)₂] states.

antisymmetrization effect in the collective mass of the kinetic term by avoiding this unfavorable condition of the $D = 0$ node.

The collective wave functions of cal(1b) and (2b) for the optional choice of the negative-parity condition are shown in Fig. 11. The condition $\Phi_{\text{coll}}^-(0) = 0$ strongly suppresses $\phi_{\text{coll}}(D)$ in the interior region and is not suitable for reproducing the GCM amplitude functions.

The collective wave functions of other calculations, cal(3), cal(4), and cal(5), are shown in Fig. 12. The differences in

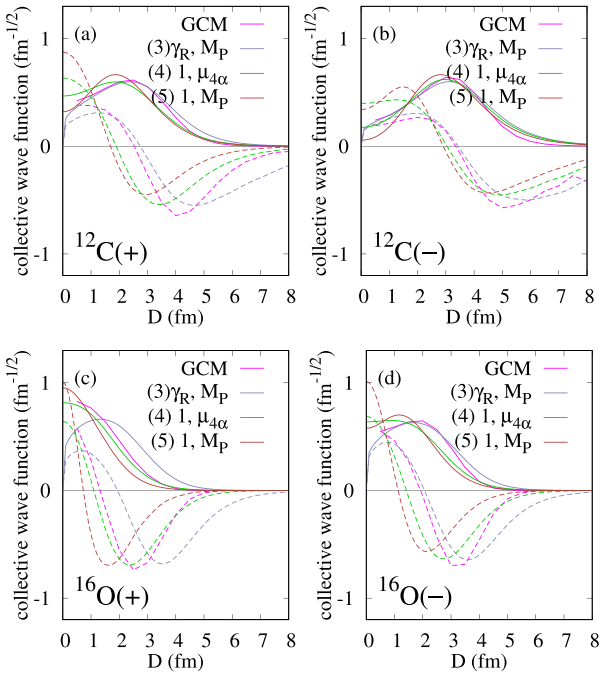


FIG. 12. Collective wave functions $\phi_{\text{coll}}(D)$ calculated by the collective models cal(3), cal(4), and cal(5) for (a) $^{12}\text{C}(+)$, (b) $^{12}\text{C}(-)$, (c) $^{16}\text{O}(+)$, and (d) $^{16}\text{O}(-)$, in comparison with the GCM amplitude function $g_{\text{GCM}}^\pm(D)$. Solid (dashed) lines indicate the functions of lower (\pm)₁ [higher (\pm)₂] states.

ϕ_{coll} of cal(3), cal(4), and cal(5) from the cal(1) and cal(2) results can be easily understood by the differences in the D dependences of γ and μ in the interior region. For example, the repulsive effect of antisymmetrization is too strong in cal(3) because γ_R is smaller than γ_N , as shown in Fig. 4, whereas it is too weak in cal(5) as expected from the enhanced $\mu = M_P$ as shown in Fig. 9.

From those analyses of the collective model calculations, it is concluded that the set $\gamma = 1$ and $\mu = \gamma_N M_P$ of cal(2) seems to be the best and simple choice among the five choices of the collective model for the global reproduction of the cluster motion obtained by the GCM. This collective model corresponds to a prescription for the derivation of the collective Hamiltonian from the energy expectation value measured by the $|D, P\rangle$ state,

$$E_P(D) = P \frac{\hbar^2}{2M_P^\pm(D)} P + E^\pm(D), \quad (27)$$

as

$$\mathcal{H}_{\text{coll}} = \left(i \frac{d}{dD} \right) \frac{1}{\gamma_N^\pm} \frac{\hbar^2}{2M_P^\pm(D)} \left(i \frac{d}{dD} \right) - T_0 + E^\pm(D), \quad (28)$$

and the matrix element of a collective operator $\mathcal{O}_{\text{coll}}$ as

$$\langle \mathcal{O}_{\text{coll}} \rangle = \int \Phi_{\text{coll}}^*(D) \mathcal{O}_{\text{coll}}(D) \Phi_{\text{coll}}(D) dD. \quad (29)$$

This model can properly describe the collective motion of $n\alpha$ systems and approximately reproduce the GCM results for the energies, radii, and amplitude functions. $\mu = \gamma_N M_P$ in the kinetic term is regarded as the effective collective mass, in which microscopic effects such as antisymmetrization and parity projection on the model space $|D\rangle$ are incorporated in the local variables $\gamma_N^\pm(D)$ and $M_P^\pm(D)$ and the dynamical effects from the Hamiltonian and finite momentum are considered in $M_P^\pm(D)$.

VI. SUMMARY

A microscopic $n\alpha$ model was applied to ^8Be , ^{12}C , and ^{16}O systems to describe the radial cluster motion in the ground and excited states. The positive- and negative-parity states were calculated with the GCM using the generator coordinate D for the $\alpha - \alpha$ distance. The cluster motion in the coordinate D space was analyzed, and the $^{12}\text{C}(+)_2$ and $^{16}\text{O}(+)_2$ states were found to be large-amplitude modes of radial excitation built on the ground states.

To describe the cluster motion of the $n\alpha$ systems, we proposed a collective model in the one-dimensional coordinate D by utilizing inputs from the parity-projected microscopic $n\alpha$ wave functions. The potential term in the collective Hamiltonian was given by the energy expectation values of the $n\alpha$ wave function at D . For the kinetic term in the collective Hamiltonian, a couple of prescriptions were tested. To take into account the antisymmetrization effects on the coordinate space D , the metric γ_N derived from the norm kernel was considered. To consider the dynamical effect, we introduced an imaginary shift $D \rightarrow D + iP/(2\hbar v)$ of the real parameter D and defined $|D, P\rangle$, in which D and P represent the coordinate and momentum of the intercluster motion in the asymp-

otic region. The mass M_P was evaluated from the energy expectation value of $|D, P\rangle$, and was utilized to incorporate the dynamical effect on the collective mass of the kinetic term in the collective Hamiltonian.

The collective wave functions of $n\alpha$ systems were obtained by solving the collective model. The results of five sets of metric γ and mass μ in the collective model were compared with the GCM results. Among the five cases, the set $\gamma = 1$ and $\mu = \gamma_N M_P$ of cal(2) was found to best reproduce the GCM results of the energy spectra, radii, and amplitude functions. This corresponds to the prescription of the collective model described in Eq. (28), in which the microscopic effects such as antisymmetrization and parity projection are incorporated in the parity- and D -dependent potential term and collective mass of the kinetic term.

One of the aims of the present work was to propose a collective model that can approximately obtain results equivalent to those derived by microscopic calculations. In the present paper, we performed the GCM calculations in restricted model space of $n\alpha$ systems within highly symmetric configurations and demonstrated that the collective models of cal(2) can approximately reproduce the GCM results. Because of the restriction of $n\alpha$ configurations, the theoretically obtained states can not necessarily be assigned to the experimental excited states. For instance, the calculated excitation energy of the $^{12}\text{C}(+)_2$ state was 14.8 MeV in the GCM result, which was much higher than that of the experimental $^{12}\text{C}(0_2^+)$ state at $E_x^{\text{exp}} = 7.65$ MeV, because the $^{12}\text{C}(0_2^+)$ state has a more complicated 3α structure beyond the regular triangle configuration. The collective model of cal(2) also provided much higher excitation energy $E_x = 13.4$ MeV of the $^{12}\text{C}(+)_2$ state consistently with the GCM calculation, which indicates the same conclusion. However, the collective model of cal(5) obtained the excitation energy $E_x = 6.8$ MeV of the $^{12}\text{C}(+)_2$ state, which eventually coincides with $E_x^{\text{exp}} = 7.65$ MeV of the experimental $^{12}\text{C}(0_2^+)$ state. It indicates a risk that an inadequate collective model could lead to an incorrect assignment of the experimental spectra, provided that the model was applied without checking its validity.

It is practically difficult to perform microscopic calculations with full model space of $n\alpha$ systems for heavier systems because of the computational cost. Therefore, it is important to extend the present collective model beyond the simple $n\alpha$ configurations and apply it to heavy systems. For further extensions to multidimensional calculations, the prescription of cal(2) proposed in the present paper may be a useful approach to incorporating microscopic and dynamical effects to the collective mass and potential energy based on the diagonal matrix elements of microscopic calculations. It is also a challenging issue to construct collective models that can be applied to various cluster dynamics in heavy systems such as cluster decay and fusion phenomena.

ACKNOWLEDGMENTS

This work was supported by Grants-in-Aid of the Japan Society for the Promotion of Science (Grants No. JP18K03617,

No. JP18H05407, No. JP22K03633, and No. JP20K03964). Discussions during the YIPQS international workshop on "Mean-field and Cluster Dynamics in Nuclear Systems" were useful to complete this work.

APPENDIX: PHYSICAL COORDINATES

In the AMD framework [19], the wave function of an A -nucleon system is written by a Slater determinant $\Phi_{\text{AMD}} = \det[\psi_i(j)]$, where the single-nucleon wave function $\psi_i(j) = \varphi_{\mathbf{Z}_i}(\mathbf{r}_j)\mathcal{X}_i(\chi_j)$ is a product of the spatial wave function and the spin-isospin function $\mathcal{X}_i = \{p\uparrow, p\downarrow, n\uparrow, n\downarrow\}$. $\varphi_{\mathbf{Z}}$ is given by a coherent state of a harmonic oscillator,

$$\varphi_{\mathbf{Z}}(\mathbf{r}) = \left(\frac{2\nu}{\pi}\right)^{4/3} \exp\left[-\nu(\mathbf{r} - \mathbf{Z}/\sqrt{\nu})^2 + \frac{1}{2}\mathbf{Z}^2\right]. \quad (\text{A1})$$

For the single-nucleon wave function, the mean position $\langle \mathbf{r} \rangle$ and momentum $\langle \mathbf{p} \rangle$ are given by the real and imaginary parts of \mathbf{Z} as

$$\langle \mathbf{r} \rangle = \mathbf{d}, \quad \langle \mathbf{p} \rangle = \mathbf{k}, \quad (\text{A2})$$

$$\mathbf{Z} = \sqrt{\nu}\mathbf{d} + \frac{i}{2\hbar\sqrt{\nu}}\mathbf{k}. \quad (\text{A3})$$

However, in the A -nucleon wave function, \mathbf{d}_i and \mathbf{k}_i indicate positions and momenta of nucleons no longer because of the antisymmetrization. Ono *et al.* [19] introduced the physical coordinates \mathbf{W}_i instead of \mathbf{Z}_i as

$$\mathbf{W}_i \equiv \sum_{j=1}^A (\sqrt{Q})_{ij} \mathbf{Z}_j, \quad (\text{A4})$$

where

$$Q_{ij} = B_{ij}B_{ji}^{-1} = \frac{\partial}{\partial(\mathbf{Z}_i^* \cdot \mathbf{Z}_j)} \ln \langle \Phi_{\text{AMD}} | \Phi_{\text{AMD}} \rangle, \quad (\text{A5})$$

$$B_{ij} \equiv \langle \psi_i | \psi_j \rangle = e^{\mathbf{Z}_i^* \cdot \mathbf{Z}_j} \langle \mathcal{X}_i | \mathcal{X}_j \rangle, \quad (\text{A6})$$

$$\langle \Phi_{\text{AMD}} | \Phi_{\text{AMD}} \rangle = \det B. \quad (\text{A7})$$

This is an extension of the physical coordinates in the 2α system proposed by Saraceno *et al.* in Ref. [20].

For the present model space of the 2α , 3α , and 4α systems, \mathbf{Z}_i is taken to be $\mathbf{Z}_i = \mathbf{S}_m/\sqrt{\nu}$ ($i \in \alpha_m$) with the real parameter \mathbf{S}_m . Because of the symmetry of spatial configurations of \mathbf{S}_m , the physical coordinates are simply given as $\mathbf{W}_i = \lambda_{n\alpha}(D)\mathbf{Z}_i$ with the scaling factors

$$\lambda_{2\alpha}(D) = \sqrt{\frac{1 + e^{-\nu D^2}}{1 - e^{-\nu D^2}}}, \quad (\text{A8})$$

$$\lambda_{3\alpha}(D) = \sqrt{\frac{1 + e^{-\nu D^2/2} + e^{-\nu D^2}}{1 + e^{-\nu D^2/2} - 2e^{-\nu D^2}}}, \quad (\text{A9})$$

$$\lambda_{4\alpha}(D) = \sqrt{\frac{1 + 2e^{-\nu D^2/2} - 3e^{-\nu D^2}}{1 + e^{-\nu D^2/2} - 2e^{-\nu D^2}}}. \quad (\text{A10})$$

- [1] D. L. Hill and J. A. Wheeler, Nuclear constitution and the interpretation of fission phenomena, *Phys. Rev.* **89**, 1102 (1953).
- [2] J. J. Griffin and J. A. Wheeler, Collective motions in nuclei by the method of generator coordinates, *Phys. Rev.* **108**, 311 (1957).
- [3] D. M. Brink, Many-body description of nuclear structure and reactions, in *Proceedings of the International School of Physics "E. Fermi"*, Vol. XXXVI, edited by C. Bloch (Academic, New York, 1965), p. 247.
- [4] D. M. Brink and A. Weiguny, The generator coordinate theory of collective motion, *Nucl. Phys. A* **120**, 59 (1968).
- [5] H. Horiuchi, Generator coordinate treatment of composite particle reaction and molecule-like structures, *Prog. Theor. Phys.* **43**, 375 (1970).
- [6] E. Uegaki, S. Okabe, Y. Abe, and H. Tanaka, Structure of the excited states in ^{12}C . I, *Prog. Theor. Phys.* **57**, 1262 (1977).
- [7] Y. Fujiwara *et al.*, Chapter II. Comprehensive study of alpha-nuclei, *Prog. Theor. Phys. Suppl.* **68**, 29 (1980).
- [8] P. Descouvemont and D. Baye, Microscopic theory of the $^8\text{Be}(\alpha, \gamma)^{12}\text{C}$ reaction in a three-cluster model, *Phys. Rev. C* **36**, 54 (1987).
- [9] M. Libert-Heinemann, D. Baye, and P.-H. Heenen, Generator-coordinate study of inelastic $\alpha + ^{12}\text{C}$ scattering, *Nucl. Phys. A* **339**, 429 (1980).
- [10] S. Saito, Interaction between clusters and pauli principle, *Prog. Theor. Phys.* **41**, 705 (1969).
- [11] P. G. Reinhard and K. Goeke, The generator coordinate method and quantised collective motion in nuclear systems, *Rep. Prog. Phys.* **50**, 1 (1987).
- [12] T. Marumori, T. Maskawa, F. Sakata, and A. Kuriyama, Self-consistent collective-coordinate method for the large-amplitude nuclear collective motion, *Prog. Theor. Phys.* **64**, 1294 (1980).
- [13] M. Matsuo, T. Nakatsukasa, and K. Matsuyanagi, Adiabatic selfconsistent collective coordinate method for large amplitude collective motion in nuclei with pairing correlations, *Prog. Theor. Phys.* **103**, 959 (2000).
- [14] N. Hinohara, T. Nakatsukasa, M. Matsuo, and K. Matsuyanagi, Microscopic derivation of collective Hamiltonian by means of the adiabatic self-consistent collective coordinate method: Shape mixing in low-lying states of ^{68}Se and ^{72}Kr , *Prog. Theor. Phys.* **119**, 59 (2008).
- [15] K. Wen and T. Nakatsukasa, Self-consistent collective coordinate for reaction path and inertial mass, *Phys. Rev. C* **94**, 054618 (2016).
- [16] D. M. Brink, H. Friedrich, A. Weiguny, and C. W. Wong, Investigation of the alpha-particle model for light nuclei, *Phys. Lett. B* **33**, 143 (1970).
- [17] A. Volkov, Equilibrium deformation calculations of the ground state energies of 1p shell nuclei, *Nucl. Phys.* **74**, 33 (1965).
- [18] Y. Kanada-En'yo, T. Suhara, and Y. Taniguchi, Approximation of reduced width amplitude and application to cluster decay width, *Prog. Theor. Exp. Phys.* **2014**, 073D02 (2014).
- [19] A. Ono, H. Horiuchi, T. Maruyama, and A. Ohnishi, Antisymmetrized version of molecular dynamics with two-nucleon collisions and its application to heavy ion reactions, *Prog. Theor. Phys.* **87**, 1185 (1992).
- [20] M. Saraceno, P. Kramer, and F. Fernandez, Time-dependent variational description of $\alpha\alpha$ scattering, *Nucl. Phys. A* **405**, 88 (1983).